Master of Science Thesis
VT2024

Investigation of Image Co-Registration for Mapping Cortical Microstructures using dMRI

Julia Alm Ekwall

Supervisors

Markus Nilsson and Nicola Spotorno

Medical Radiation Physics, Lund
Medical Physics Programme
Faculty of Science
Lund University, Sweden
www.msf.lu.se

Populärvetenskaplig sammanfattning

Alzheimers sjukdom är idag den vanligaste neurodegenerativa sjukdomen i världen. Det klassas som en ålderssjukdom, och med en ökande medelålder i befolkningen, ökar således risken för fler att drabbas. Sjukdomen orsakar en förtunning av hjärnvävnad och presenterar sig med symptom så som minnesstörningar som gradvis blir värre. Symptomen av Alzheimers sjukdom kan däremot uppkomma så sent som flera år efter att sjukdomen har börjat bryta ned hjärnan. På grund av det så finns det ett behov och motivation för att hitta indikationer av Alzheimers sjukdom i en befolkning under ett tidigare skede. Detta för att kunna påbörja behandling tidigare men även för att möjliggöra en övervakning av sjukdomsförloppet för att fördjupa kunskaperna om sjukdomen. Det som faktiskt sker i hjärnan är att neuroner dör, vilket orsakar en mikrostrukturell förändring i de drabbade områdena. Orsaken till varför detta sker är dock ännu inte fastställd. Denna förändringen i hjärnan visar sig dock vara mätbar med magnetresonanstomografi (MRT) eller mer specifikt diffusions MRT.

Det finns däremot begränsningar av upplösningen i bilder som producerats med diffusions MRT. Upplösningen är för låg för att kunna urskilja mindre strukturer i bilden och istället blir det man ser påverkat av så kallade partiella volymseffekter (PVE). PVE innebär att strukturerna även innehåller information från omkringliggande strukturer, för att upplösningen inte är hög nog för att urskilja dem. Då ändringarna i hjärnan orsakade av Alzheimers sjukdom sker på en mikroskopisk nivå så behöver mätmetoderna vara mer exakta. En lösning på det problemet är att man använder sig av bildregistrering. En bildregistrering innebär att man för över en diffusionsbild in i rymden av en högre upplöst bild, exempelvis en T1-viktad MRT-bild. Om bilderna befinner sig i samma rymd kan man dra nytta av den högre upplösta bilden för att öka upplösningen av diffusionsbilden. Detta kommer då resultera i att de partiella volymseffekterna upplevs som mindre. Bildregistrering är däremot en metod i sig som kräver optimering. Det finns många olika sätt en bildregistrering kan utföras på men vilket sätt som är det bästa är ännu okänt. Utvärderingsverktyg som evaluerar prestandan i bildregistreringen finns det också ett behov av. Således har syftet med detta arbetet varit att jämföra olika metoder för registrering för att eventuellt komma fram till en metod som ger oss en bildregistrering med bästa möjliga resultat. Förrutom det så har syftet även varit att hitta ett sätt att utvärdera registreringarna på.

De olika metoderna för att utföra en registrering på som har utvärderats i detta arbetet är: rigid, affine, nonlinear (ickelinjär) och combined som är en kombinerad metod (innehållande en rigid, affine och slutligen en ickelinjär transformering). Dessa metoder skiljer sig från varandra i hur de anpassar positioneringen av diffusionsbilden gentemot den högre upplösta bilden. I detta arbetet utvärderades även skillnaden i resultat när registreringarna använde diffusionsbilder med olika konstraster (olika b-värden) för att genomföra (driva) registreringarna. Kontrasterna som användes bestod av ett lågt b-värde (b0), vilket ger en bild med hög signal och därmed områden med hög intensitet. Ett högt b-värde (b2500) användes också, vilket ger en bild med lägre signal och mindre intensitetsskillnader i bilden. Utvärderingen av registreringsmetoderna har bestått av visuell evaluering samt evaluering av fördelningen av medeldiffusiviteten i hjärnbarken i form av PVE-index.

Resultatet av den visuella evalueringen visade att det fanns en skillnad mellan de olika undersökta metoderna för att utföra en registrering på. Resultaten av PVE-indexen visade på att combined presterade sämst utav metoderna som utvärderades. I fallen när b0 drev registreringarna så visade resultaten att rigid resulterade i det minsta PVE-indexet. När b2500 drev registreringarna så visade resultaten istället att registreringarna med transformerna rigid, affine och nonlinear presterade likvärdigt. Resultaten visade även på att det fanns en skillnad mellan när b0 och b2500 drev registreringarna.

Abstract

Introduction and aim

The changes in the brain caused by Alzheimer's disease usually begin many years before the first symptoms arise. The effect of the neurodegenerative disease involves both morphological and microstructural changes in the brain, due to neurons dying. These changes in the microstructure can be measured with diffusion MRI. The resolution however limits the accuracy of the imaging, making structures more difficult to distinguish due to partial volume effects (PVE). PVE occurs when voxels contain information from multiple tissues, which takes place more frequently when the resolution is low. To reduce the PVE the diffusion-weighted image (DWI) can be registered to a T1-weighted image. The registration enables the use of a segmentation of the gray and white matter from the T1-weighted image. This segmentation can be used on the DWI to measure changes in the microstructure of the brain. There are however many ways to register images, therefore there is a need to identify which method of registration that produces the best alignment between images with the least influence of PVE. There are additional steps on how to reduce the PVE, such as using a Bowsher prior method where the registered diffusion images are reconstructed into a higher resolution.

Material and Methods

Registrations were performed in different ways by using the different transforms rigid, affine and nonlinear. A combined method with multiple input images was also used to perform a registration in this work. The registrations were alternately driven by a b0-image or a b2500-image. The b0 and b2500 are images with different contrasts, where the b0 has a low diffusion weighting and the b2500 has a high diffusion weighting. The registrations were evaluated by visual evaluations and by extracting mean diffusivity (MD) values from the cortex. The MD-values in the cortex range up to approximately $1.1 \cdot 10^{-3}$ mm^2/s for a cognitively normal individual. Values higher than this occur due to PVE with the cerebrospinal fluid (CSF) surrounding the cortex. The fraction of voxels in the cortex with an MD-value above $1.1 \cdot 10^{-3}$ mm^2/s was therefore used as a PVE-index. Furthermore, the distribution of PVE-indices was evaluated in 70 cortical regions which were extracted with the Desikan–Killiany atlas available in FreeSurfer. A reconstruction of the registered diffusion-weighted images was also performed with the Bowsher prior method.

Results

The registrations showed a notable difference in the visual evaluations, especially when the b0 was driving the registrations. From the evaluation of the PVE-index, the results indicated that it was superior to drive the registration with the b2500 instead of the b0. A paired t-test confirmed that there was a statistically significant difference between driving the registrations using either the b0 or the b2500. The PVE-indices varied between different registrations as well. The difference was more notable between registrations when the b0 was used in comparison to the b2500. A two-way ANOVA without reproducibility showed a statistically significant difference between registrations for both b0 and b2500 driving the registrations. The ANOVA was followed up with Tukey's post hoc honestly significant difference (HSD) test. It showed a statistically significant difference between all registrations when the b0 was used. For when the b2500 was driving the registrations, all registrations showed a statistically significant difference except for between the rigid and affine and between the affine and nonlinear transforms. The reconstructed diffusion images with the Bowsher prior method resulted in a visually higher resolution. The algorithm however altered the values in the images which prevented further evaluation of this approach.

Conclusion

The results indicated that the rigid transform produced the highest registration accuracy when the b0 was used to drive the registrations. When the b2500 was used to drive the registrations, the accuracy of the registrations increased and the result suggested that the accuracy was similar for rigid, affine and nonlinear. The result also indicated that the analysis of registration accuracy is not straightforward.

Abbreviations

AD	Alzheimer's disease
ANTs	Advanced Normalization Tools
BET2	Brain extraction tool
CC	Cross correlation
cn	Cognitively normal
CSF	Cerebrospinal fluid
CT	Computed tomography
dMRI	Diffusion magnetic resonance imaging
DWI	Diffusion weighted image
FA	Fractional anisotropy
HSD	Honestly significant difference
mci	Mild cognitive impairment
MD	Mean diffusivity
MI	Mutual information
MMORF	Multimodal registration framework
MRI	Magnetic resonance imaging
PET	Positron emission tomography
PSF	Point spread function
PVE	Partial volume effects

Contents

1 Introduction

Alzheimer's disease (AD) is the most common neurodegenerative disease in the world [1]. It is characterized by the accumulation of amyloid-β plaques in the extracellular space [2]. The buildup of this protein can begin 10-20 years before the first symptoms arise such as memory impairment. Tau tangles are additionally a characterization of AD which forms within neurons. The buildups of these proteins cause neuronal death and atrophy in the brain [3]. Diffusion MRI (dMRI) is a quantitative measure that can provide information about the microstructure of tissues [4]. The microscopic information can be gathered due to its sensitivity to the random motion of water molecules [5]. Studies have implied that dMRI, and more specifically the mean diffusivity (MD) can be used as an indication of changes appearing in the microstructure [4, 6]. Studies then show that the mean diffusivity could be used to indicate early signs of neurodegeneration and it appears to enable indications of an early-stage Alzheimer's disease in a population [7].

There is a great need to find ways for an early diagnosis [2]. It does not only revolve around an accurate treatment of the disease, which is important to begin with as soon as possible but also for the patient's sake. It is important for them to know, understand and be able to prepare for what is to come. Additionally, there is a great need to learn more about the progression of the disease, meaning that the results of the measurements are required to be more accurate revolving follow-up imaging of patients. Furthermore, that becomes relevant in the determination if treatments are working or not. The relevance increases further as medicine evolves, which might make therapies an available option in the future [2].

Although the dMRI makes for a promising method for finding indications of an early stage AD in a population, it has some limitations. The resolution of the dMRI, which usually is around 2x2x2 mm^3, is currently too low. Alzheimer's disease often appears in the memory-forming regions of the brain, such as the hippocampus and different regions of the cortex [3]. The cortical thickness is approximately 2.5 mm and the average volume of the hippocampus is just below 4 cm^3 [8, 9]. This means that important structures that could contain information about an early ongoing AD are approximately the same size as the resolution of the diffusion-weighted images (DWIs). Therefore the images will be influenced by partial volume effects (PVE) from the surrounding tissues such as the cerebrospinal fluid (CSF). The true result will thus be obscured because of the partial volume effects, leading to poor accuracy in the measurement of the MD [10]. The poor accuracy will lead to difficulties in differentiation between PVE and true measurements.

The current limitations may however be bypassed by co-registering the diffusion-weighted image to an image with a higher resolution. By using co-registration, the image with the higher resolution, which can be a T1-weighted image, can be used for a more accurate orientation in the image with lower resolution. The higher resolution image can also be used for segmentation of important regions that correspond to the same regions in a lower resolution image after the images are registered to one another [11]. A spatial alignment of the images with a registration would imply that a point in the higher resolution image would correspond to the same one in the diffusion-weighted image. An accurate registration would then decrease the influence of the PVE. However, there are many ways to perform a registration involving different algorithms, transformations of the images and implementations [12]. Hence the outputs of the registrations will differ when using different implementations. However all registrations have the same goal, and that is to spatially align the images. Therefore it becomes important to determine the accuracy of the alignment for respective registration [12]. The accuracy needs to be sufficiently high to reduce the influence of the partial volume effects that disturb the measurements of the mean diffusivity in the cortical regions.

1.1 Aim

This project aimed to investigate combinations of different implementations of co-registrations to increase the resolution of the DWI. There is a need to determine which way of performing a registration would result in the most accurate registration that decreases the influence of the PVE the most, which disturbs current measurements of the mean diffusivity in the cortical regions. The purpose also included finding a way to quantify the accuracy of the registration between the diffusion-weighted image and the T1-weighted image. A higher accuracy would thus contribute to enabling accurate indications for early signs of Alzheimer's disease

in a population. A reconstruction algorithm, the Bowsher priors, which increases the resolution of an image was also investigated to decrease the influence of the partial volume effects after the registration.

2 Theory

2.1 Alzheimer's disease

Alzheimer's disease is the most common neurodegenerative disease today and studies show that 20% of women and 10% of men will get AD in their lifetime [2]. It most commonly appears among older individuals, and with an increasing life expectancy in countries, the disease is expected to become more common. Alzheimer's disease is characterized by the accumulation of amyloid-β plaques in cortical extracellular space [2]. The buildup of this protein can begin 10-20 years before the first symptoms arise. Due to the symptoms appearing years later, the disease is difficult to find in an early stage. Common symptoms among affected individuals are memory impairment due to AD affecting the cortical regions and the hippocampus [3]. Besides amyloid-β plaques, another way to characterize AD is by the spread of tau tangles which form within neurons [2]. The unhealthy buildup of these proteins has consequences such as neuronal death and atrophy in the brain [3], which is illustrated in figure 2.1. During the progression of the disease, the symptoms will become more severe due to increased atrophy.

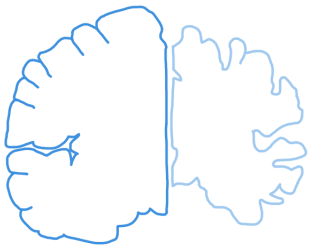

Figure 2.1: An illustration of how the changes in the brain appear in Alzheimer's disease. The left side resembles a cognitively healthy brain whilst the right side resembles AD with severe atrophy.

The cause of the disease is not entirely known but seems to be a combination of factors such as genetics, lifestyle and changes in the brain caused by aging. Currently, there are a lot of ongoing studies regarding dementia specifically Alzheimer's disease. There is a great need to develop biomarkers that can track the progression of the disease and the response to treatments [7]. For instance, the buildup of proteins associated with Alzheimer's disease is currently being investigated with the use of positron emission tomography (PET) [2]. Furthermore, studies have shown indications that the mean diffusivity can be used as an indication of early-stage Alzheimer's disease in a population [7].

2.2 Diffusion

Diffusion MRI is based on the effects of the Brownian motion of water in the human body, where the Brownian motion is the random displacement of microscopical particles [13]. The basic principle regarding diffusion MRI is by first applying a gradient (external magnetic field) which will defocus the magnetization vectors (spins) [5]. Then after a short period, the same gradient is applied in the opposite direction, causing the spins to refocus again and the signal to increase. However during this time when the gradient is applied, some of the spins will have been displaced due to the Brownian motion and will thus not be refocused by the second gradient due to their new location. This will cause the total signal to decrease, hence more diffusion implies less signal. The following formula describes the relationship between the signal depending on the diffusion weighting of the image [13]

$$S = S_0 e^{-bD}. \tag{2.1}$$

Here S is the output signal of the image, S_0 is the signal without any diffusion gradients applied and D is the diffusivity. The diffusivity describes the apparent diffusion measured in the scan. Lastly, b is a value that

gives a measure of how large the diffusion weighting on the image would be. The b-value formula is described as follows

$$b = \gamma^2 G^2 \delta^2 (\Delta - \frac{\delta}{3}), \tag{2.2}$$

where γ is the gyromagnetic ratio, G is the magnitude of the gradient, δ is the duration of the applied gradients and Δ is the time between gradient pulses [13]. Thus, larger b-values imply an increase in any of the parameters from equation 2.2, resulting in a higher diffusion-weighted image, but also less signal according to equation 2.1.

2.2.1 Diffusion tensor imaging

The Brownian motion is a random displacement of microscopical particles. The displacement can occur in any direction, and that can be analyzed with diffusion tensor imaging (DTI). The movement of the particles is limited due to the surrounding structures such as axons, neurons and other tissues in the brain. This will result in some sort of directionality of the measurement, called anisotropic diffusion [14, 15]. There will be a direction where the diffusivity would be faster, for instance along an axon in comparison to the diffusivity in other directions within the axon, which thus will be lower. The diffusion tensor can be expressed by a 3x3 matrix with 3 orthogonal eigenvectors and 3 positive eigenvalues (λ_1, λ_2, λ_3) [14]. Due to the anisotropy, there will be a preferred direction of the diffusivity, which is described by the major eigenvector with its respective major eigenvalue that describes the degree of the diffusivity [14, 15]. The diffusion tensor can be helpful in many ways in medical imaging, for instance, the anisotropy can be used to calculate the fractional anisotropy (FA) which can be used when it comes to grading glial tumors [15].

2.2.2 Mean diffusivity

Besides FA, other useful parameters can be derived from diffusion tensor imaging, for instance, the mean diffusivity (MD). MD could be calculated from the eigenvalues by simply taking the arithmetic average of them [15]. It thus describes the average of the diffusivity in all directions in different areas. A high MD would imply a high mobility of the water molecules. This in turn could be used as a measurement of changes in the microstructure in the human body. Studies have shown indications that the mean diffusivity can be used as an indication of early-stage Alzheimer's disease in a population [16, 17].

2.3 Image resolution

The resolution in an image describes the smallest distance in which two points can be distinguished. There is a relationship between image resolution and the point spread function (PSF), which states that the two points can be distinguished if they are separated at a minimum distance of the full width at half maximum (FWHM) of the PSF [18]. To increase the image resolution, more information needs to be collected during the measurements i.e. There has to be a higher sampling density. The resolution of an image is however limited in many aspects which can be time or field of view (FOV) for instance.

2.4 Image registration

There is a variety of different techniques available today for medical imaging, for instance, magnetic resonance imaging (MRI), computed tomography (CT) and PET. They allow different perspectives in viewing the anatomy of a patient, and combined they contribute to comprehensive information about the imaged volume. However, to combine the images from the different modalities, there has to be a processing step of the images to align them. This is usually not straightforward considering that the techniques differ from one another and therefore the spatial information in the images differ as well. Because of this, a spatial alignment between the images has to be performed, resulting in a voxel-to-voxel alignment before any conclusions about the information in the images from the different modalities can be drawn [19]. The same process has to be used when comparing different techniques within the different modalities, for example, different pulse sequences in MRI which results in images of different contrast.

The principle behind the registration framework revolves around a moving image $I_m(x)$ and a reference image $I_r(x)$ where the goal is to align $I_m(x)$ to $I_r(x)$ by transforming it [19]. This brings the images into

the same coordinate system which is useful when there is a need to compare or even integrate the images and the information they contain. Hence, the registration problem is solved when a transformation map that spatially aligns $I_m(x)$ to $I_r(x)$ is found. The basic principle of a registration can be seen in figure 2.2.

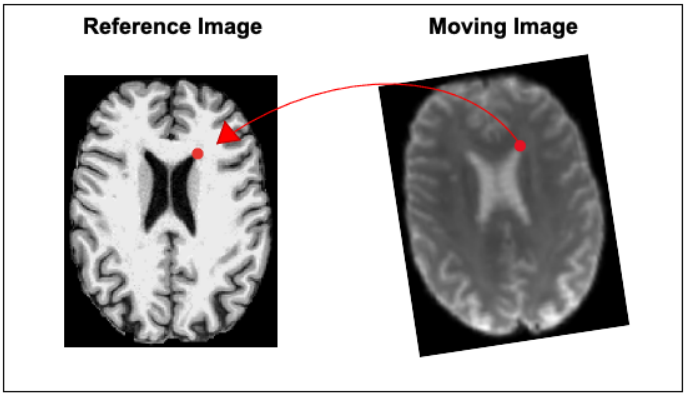

Figure 2.2: An illustration of the principle behind a registration. A point in the moving image $I_m(x)$ corresponds to a point in the reference image $I_r(x)$, but $I_m(x)$ has to be transformed for the anatomies to overlap correctly in the two images.

The framework that is used to perform a registration contains different interpolations, metrics, transforms, optimization methods and more which are needed to be able to align a point in one image to the same one in another [19]. Where for instance the optimization method, optimizes the metric so that there will be a high similarity between $I_r(x)$ and $I_m(x)$. There are many interpolation methods, metrics and transforms available, which will be discussed later. At some point the moving image is considered to be similar to the reference image, that is when the registration is completed.

2.4.1 Interpolation

The interpolation method is partially used to get the moving image on the same grid size as the reference image since they differ in some cases. It is also used in combination with the transform step in the registration, which makes it useful for the step when the transforms are applied. It is then used to find the best estimation of what the voxel values in the different regions should equal. Different interpolation methods can be used during the registration process where common ones are nearest neighbor, linear and B-spline interpolation [19]. They vary in quality for the output image and they are beneficial to use under different circumstances. The nearest neighbor is supposedly an easy interpolation method that considers the values of the surrounding voxels and performs an estimation of what the output value in the central voxel should be [20]. A linear interpolation performs a linear weighting depending on the surrounding voxels. Lastly, the B-spline interpolation works similarly to the linear one but can perform interpolation between voxels in higher orders as well.

2.4.2 Metrics

In image registration, there is also a need for a metric that measures the similarity between the image values. There are different metrics available that work in different ways, constructed by different algorithms. A sufficient similarity between the images is reached when the metric converges to a predefined value [21]. If the changes in the metric value become arbitrarily small between iterations, the moving image is considered to be similar to the reference image. Two of the more common ones to use in image registration are mutual information (MI) and cross correlation (CC) [22], but that can differ depending on which registration software is used [21]. An example of a software that can be used to perform registrations is the Advanced Normalization Tools (ANTs).

Cross correlation performs calculations in neighbourhoods over $I_m(x)$ and $I_r(x)$. The cross-correlation method in equation 2.3 is similar to approaches used for image filtering [23]. From ANTs, the CC func-

tion can be expressed as the following

$$CC(x) = \frac{\sum_i \left(\left(I_m(x_i) - \mu_{I_m(x)} \right) \left(I_r(x_i) - \mu_{I_r(x)} \right) \right)^2}{\sum_i \left(I_m(x_i) - \mu_{I_m(x)} \right)^2 \sum_i \left(I_r(x_i) - \mu_{I_r(x)} \right)^2}, \tag{2.3}$$

where x is the center of a square neighborhood which is iterated over x_i. The mean of the neighborhood is denoted as μ and the $I_m(x)$ and $I_r(x)$ remain as the moving image and reference image respectively.

Mutual information is a metric that assumes a probability distribution of the two images and creates a joint histogram with the intensities from $I_m(x)$ and $I_r(x)$ [19, 23]. Hence it measures the information that is shared between two groups. It is easy to use, as well as CC, and it is described as a good metric for image registration [19]. The MI function can be expressed as the following

$$MI(\mu; I_r, I_m) = \sum_{m \in L_m} \sum_{r \in L_r} p(r, m; \mu) log_2 \left(\frac{p(r, m; \mu)}{pR(r) pM(m; \mu)} \right), \tag{2.4}$$

where L_m and L_r describes the bin centers or the sets, p the discrete joint probability and pR and pM the marginal discrete probabilities [19].

2.4.3 Transforms

Geometrical transforms are applied on the moving image $I_m(x)$ so that it will converge into a similar appearance, as well as in the same coordinate system, as the reference image $I_r(x)$. There are different ways to perform a transformation on an image. The most common ones are translation, rotation, scaling and shearing [19], which is illustrated in figure 2.3. The translation transform is used to adjust the image in the x, y and z-direction. The rotation allows it to rotate in every direction, the scaling adjusts the size of the image. Lastly, the shearing transform skews $I_m(x)$ to better resemble the $I_r(x)$. There are also nonlinear approaches that can perform transformations to $I_m(x)$ that are nonlinear to resemble $I_r(x)$. A nonlinear transformation thereby contains numerous amount of degrees of freedom.

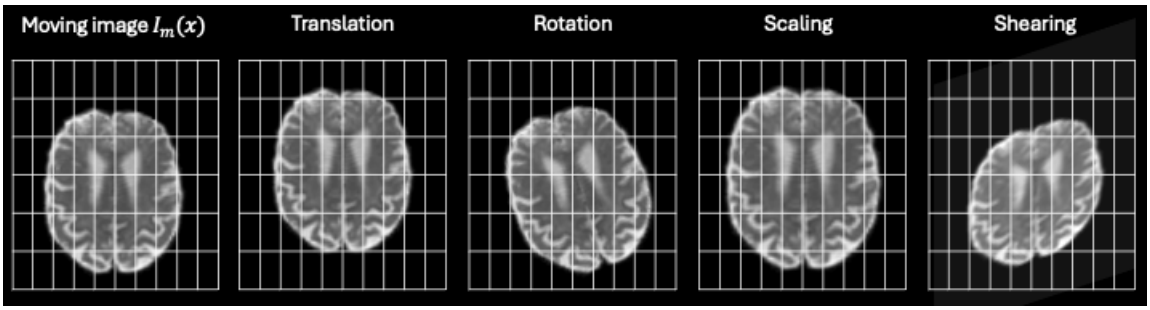

Figure 2.3: An illustration of common geometrical transformations that can be applied on the moving image $I_m(x)$ to align with the reference image $I_r(x)$, including translation, rotation, scaling and shearing.

The combination of different geometrical transformations, results in common transforms used during a registration. The combination of the transform translation and rotation results in a rigid transform. The combination of all transformations in figure 2.3, results in an affine transformation. The rigid, affine and nonlinear transforms are commonly used in the alignment of the diffusion image to a morphological image in a registration process. The translation transform can be expressed as the following [19]

$$T_\mu(x) = x + t, \tag{2.5}$$

where $T_\mu(x)$ describes the transform of $I_m(x)$ regarding to $I_r(x)$. The vector t is the translation vector and x is the voxel value. By including the rotation in the equation as well, the following formula would resemble a rigid transform, consisting of 6 degrees of freedom. The rigid transform can thus be expressed as the following

$$T_\mu(x) = R(x - c) + t + c, \tag{2.6}$$

where R is the rotation matrix and c describes the center of the rotation of $I_m(x)$. The affine transformation however consists of 12 degrees of freedom which is twice the amount as for rigid. The transformation matrix A for the affine transform thus has fewer restrictions on how it can linearly transform the moving image, in comparison to the rigid transform. The definition of an affine transformation is expressed as the following [19]

$$T_\mu(x) = A(x - c) + t + c. \tag{2.7}$$

A nonlinear transformation can perform transformations on the moving image that have no limits. A nonlinear registration, B-spline, can be expressed as the following [19]

$$T_\mu(x) = x + \sum_{x_k \in N_x} p_k \beta^3 \left(\frac{x - x_k}{\sigma} \right), \tag{2.8}$$

where x_k are control points, limiting the transformations of the image so that only required transformations are performed. N_x is the domain from which the control points are defined, p_k is defined as the B-spline coefficient vectors. β^3 is the third degree B-spline and σ is the spacing between the control points [19]. There are other options regarding nonlinear transforms, where common ones are available for instance in ANTs are B-splineSyN and SyN. The options between different transforms are generally many. The transforms could essentially be similar, but contain differences in the design of the algorithms, thereby producing transformations with different results. The choice of the transformation also has a software dependence where software-specific transformations are available as well.

2.4.4 Other registration techniques

A registration containing the nonlinear transformation can be performed in another way which can be referred to as a combined method. A combined method uses multiple scalar images as inputs to perform the transformations. The multiple scalar images can be different b-images. The registration is therefore based on the transformations on all b-images since they are all registered to the T1-space at the same time during the registration. The registration framework initiates by roughly aligning the images before the nonlinear transformation is applied to all scalar images. Due to the multiple moving images as well as transformation steps, a combined registration approach can be time-consuming.

2.4.5 Evaluation methods

The accuracy of the image registration needs to be investigated by some method of evaluation. This is a particularly important step regarding the image registration. That is because the evaluation can clarify to what extent the results could be used and where limitations in the registration are. Anatomical regions need to overlap between the registered images for it to be considered successful. A way of determining the accuracy of the registration is thus by measuring this overlap by segmenting regions in the registered images. The accuracy can then be calculated with a similarity measurement called the Jaccard metric [23]. It can be described by the following expression

$$J(I_r(x), I_m(x)) = \frac{|I_m(x) \cap I_r(x)|}{|I_m(x) \cup I_r(x)|}, \tag{2.9}$$

where the numerator describes the intersection between the volumes and the denominator the union of the volumes. The Jaccard metric measures the difference in the size of for example two binary inputs. It results in a similarity that ranges from 0 to 1, where 1 equals a perfect agreement between the inputs. Another common similarity metric that can be used is the Dice coefficient [12]. It can be expressed as the following

$$\text{Dice} = \frac{2|I_m(x) \cap I_r(x)|}{|I_m(x)| + |I_r(x)|}, \tag{2.10}$$

where the expression is similar to the Jaccard metric. The two similarity metrics are thus similar, and a scaling of one another. Depending on the purpose of the registration, the evaluation methods could be adapted according to the purpose as well.

2.5 Bowsher priors

There are ways to increase the resolution of the DWI further, by using using Bowsher priors for instance [24]. The Bowsher prior is a reconstruction method commonly applied in the case of anatomy-guided regularized PET due to the low resolution in the images. MRI images, containing a higher resolution, are used in the reconstruction of the PET images to reduce the noise and improve the resolution [24]. The reconstruction algorithm can be implemented in other modalities as well and a method where the Bowsher prior is based on the l_1-norm could be investigated for MRI images in this case instead. The images are iteratively reweighted during the reconstruction to overcome the limits of the Bowsher prior that is based on the l_2-norm, which suffers from over-smoothing. The following expression describes the l_1 Bowsher prior

$$R_{l_1}(x|z) = \sum_j \sum_{l \in N_j} W_{lj}|x_l - x_j|, \tag{2.11}$$

where the absolute value represents the l_1-norm. In this case, x would be the registered diffusion-weighted image and z the T1-weighted image. N_j is the neighbouring voxels of the j-th voxel and W_{lj} is the weighting of the difference of x_l which is the center voxel of the neighbourhood voxels x_j [24].

3 Materials and Methods

3.1 Overview

The data used for this project was acquired from the Swedish study BioFINDER-2. The data consisted of 50 individuals, where half of them were cognitively normal (cn) and the other half had a mild cognitive impairment (mci). The imaging took place at the same 3T MAGNETOM Prisma (Siemens Healthcare) in Lund, Sweden for all individuals to eliminate the variation between scanners. The scanner was equipped with a 64-channel head coil and a single-shot echo planar imaging (EPI) sequence was used to gather 104 diffusion-weighted imaging volumes. The repetition time used was: 3500 ms, echo time: 73 ms, resolution: 2x2x2 mm^3, field of view (FOV): 220x220x124 mm^3. The ranges of b-values were: 0, 100, 1000 and 2500 s/mm^2 and they were distributed over 2, 6, 32 and 64 directions. A two-fold parallel acceleration and partial Fourier factor of 7/8 were used. For the structural image, a T1-weighted MPRAGE (magnetization prepared rapid gradient echo) sequence was acquired. The following acquisition parameters were used: inversion time: 1100 ms, flip angle: 9 degrees, echo time: 2.54 ms, echo spacing: 7.3 ms, repetition time: 1900 ms, receiver bandwidth: 220 Hz/pixel, voxel size: 1x1x1 mm^3. GRAPPA (generalized autocalibrating partially parallel acquisitions) was also applied with an acceleration factor of 2 and 24 reference lines.

3.2 Preprocessing

The structural data was preprocessed using FreeSurfer (version 6.0, `https://surfer.nmr.mgh.harvard.edu`). The pipeline consists of, for instance, segmentation of grey and white matter as well as skull-stripping and homogeneity correction. It also included the Desikan–Killiany atlas from which cortical regions could be extracted. The diffusion-weighted images were corrected for susceptibility by taking advantage of the reversed phase encoding directions that the data was collected in. FSL (FMRIB Software Library, version 6.0.4; Oxford, UK) was used for motion and eddy current correction.

3.3 ANTs

The software used to run the registrations was Advanced Normalization Tools (ANTs). The software is useful in both registrations but also in some preprocessing with, for example, bias correction [25]. There are other software available to run registrations with besides ANTs as well. The software has differences in for instance the algorithms, metrics, sampling methods, transformations, etc. Different results would thus be expected from using different software in performing the registrations.

3.4 Registration

An additional step of preprocessing had to be performed on the data before the registrations could be initiated. The diffusion-weighted images were used to extract b-values images (scalar images) from. The b-value images extracted were: b0, b1000 and b2500. Thereafter the images were averaged resulting in an average of b0, b1000 and b2500 respectively. This process can be observed to the left in figure 3.1. A brain mask of the b0 image was then created to skull-strip the data. The brain mask and skull-stripping of the data were performed using the brain extraction tool (BET2) in FSL [26, 27]. The brain mask was then applied to the other diffusion scalar images as well. The entire process described above can be observed in figure 3.1.

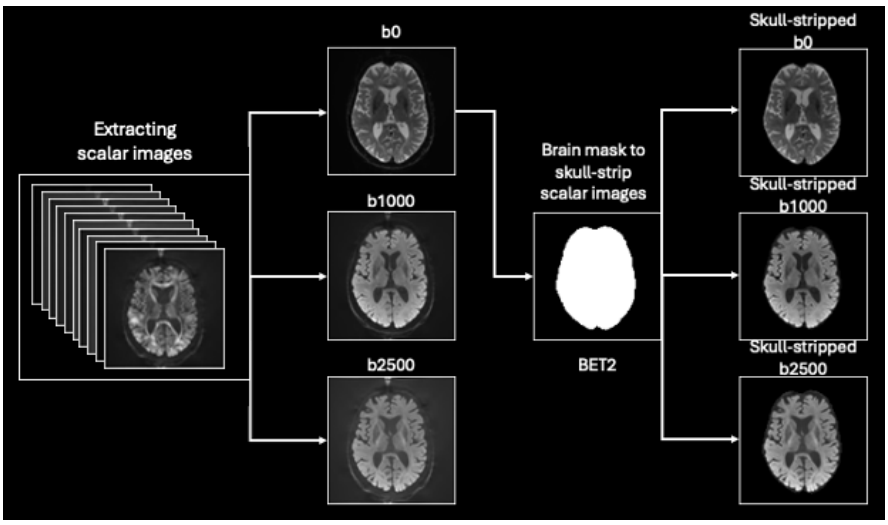

Figure 3.1: An illustration of the process of preparing the data for registration. The scalar images were extracted from the DWI to the left in the figure and then averaged, resulting in three averaged scalar images b0, b1000 and b2500. Thereafter the brain mask was created with BET2 from the averaged b0, which was used to skull-strip the scalar images. The skull-stripped images can be seen to the right in the figure.

Tensor images were thereafter created from the skull-stripped scalar images by using Mrtrix3 (Mrtrix3, `https://www.mrtrix.org/`). From the tensor images, mean diffusivity maps were created as well.

The registrations were all performed with ANTs [25]. The averages of the b0 and the b2500 images were both used as moving images $I_m(x)$ to run the different registrations, which can be seen in figure 3.2. This was to be able to compare the results of the registrations depending on which moving image that was used to drive the registrations. Thus in all registrations, a DWI, either the b0 or the b2500, was registered to the T1-weighted image and brought into that space, joining the coordinate systems of the images. Three different transforms were used for the registrations consisting of a rigid, affine and nonlinear transform. A combined method was also investigated in this work, consisting of three b-images as inputs, the b0, b1000 and the b2500. Thus, in total, four different ways of performing registrations were investigated which differed from one another in the implementation of the registration. They are referred to as rigid, affine, nonlinear and combined in this work. The registration framework for the combined also consisted of multiple transforms. It included a rigid and an affine transform before a nonlinear transform lastly was performed to complete the transformation. The details concerning how the registrations were performed with respective method can be observed in Appendix A. After the registrations were performed, the mean diffusivity images created from the tensor images were brought into the same coordinate system as the DWI and the T1-weighted image. This was performed by applying the same transformation performed during the registrations. Details concerning this can also be found in Appendix A.

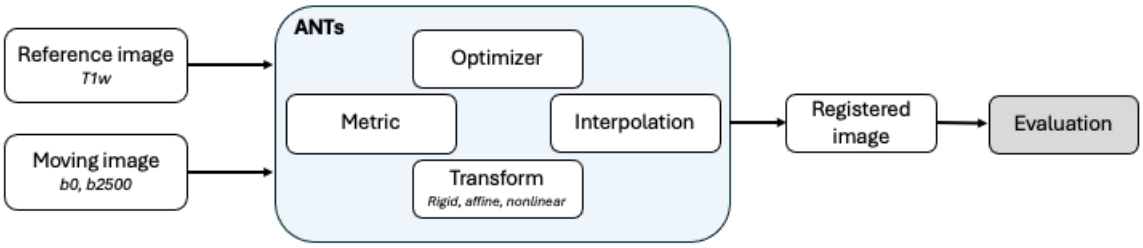

Figure 3.2: An illustration of the essential components in the registration process used in this work. To the left in the figure, the input images can be observed where both the b0 and the b2500 images were used as moving images. In the center, a representation of the registration performed by ANTs can be observed. It includes a rigid, affine and nonlinear transformation which was used in this work. The output from ANTs is a registered image which will continue to the last step in the figure, consisting of an evaluation of the registration accuracy.

3.5 Evaluation

The accuracy of the registrations was evaluated with four different methods including a visual evaluation, difference maps, PVE-indices in the cortex and PVE-indices across cortical regions.

3.5.1 Visual evaluation

A visual overview initiated the evaluation process of the different registrations. This was first performed in a viewer in FSL, where the images were overlayed to compare the registration accuracy in the different regions of the brain volumes. Regions where the registration was expected to have a lower accuracy were observed a bit closer, such as the frontal lobe. That is because susceptibility artifacts are common in the anterior parts of the brain and preprocessing only removes the majority of these artifacts. An example of susceptibility artifacts and the results of the preprocessing can be seen in figure 3.3. This visual evaluation was used to get an indication of the accuracy of the different registration methods and to get a better understanding of their performance.

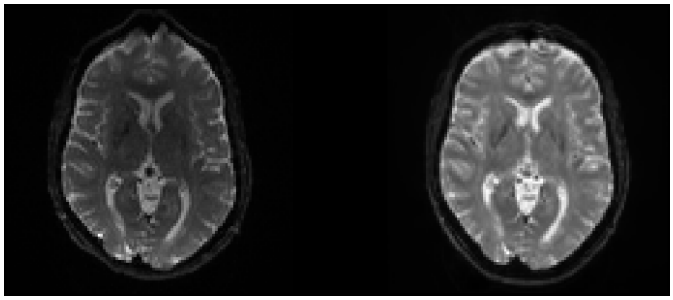

Figure 3.3: Susceptibility artifacts can be seen in the anterior parts of the brain in the DWI to the left. To the right, a b0-image can be observed of the same individual and slice after preprocessing with FSL.

The visual evaluation was then elaborated by outlining a part of the cortex in the T1-weighted image for comparison between registrations. The outlining was performed in a slice of the anterior and posterior part of the T1-weighted image. Thereafter the outlining was applied to the MD-maps in the T1-weighted space, driven by b0 and b2500 respectively. The outlining then acted as a barrier, indicating the correct placement of the cortex concerning the T1-weighted image. Due to this, a comparison between different registrations was feasible. The outlining was performed in Matlab (MATLAB R2023b, The MathWorks Inc, Natick,

Massachusetts) with code used from GitHub (`https://github.com/markus-nilsson/md-dmri`). Due to the common occurrence of susceptibility artifacts in the anterior parts of the brain, the outlining could also indicate how the different registrations managed the residual artifacts left after the preprocessing.

3.5.2 Difference maps

The second evaluation method consisted of creating difference maps that would highlight regions of low accuracy in the registrations. Before a subtraction of the DWI and the T1-weighted image could be performed, the image intensities had to be made similar in the images. This was performed by scaling the intensities in the DWI with the intensities in the T1-weighted image. The T1-weighted image was first Gaussian smoothed with a width of 1 before the intensities were extracted from it for the scaling of the DWI. The b2500 image was used for the difference maps due to the contrast already being similar to the contrast of the T1-weighted image. After the intensities of the DWI had been scaled with regard to the intensities in the T1-weighted image, the difference maps were created by performing a subtraction between the T1-weighted image and the DWI. If the accuracy of the registrations is performed perfectly, the result of the subtraction would be a homogeneous image. The difference maps of the different registration methods were then compared to one another. This evaluation method could be used as an indication of regions where respective registrations had a low respectively high accuracy. Although this evaluation method was computed, it resulted in another visual evaluation method as well.

3.5.3 PVE-indices in the cortex

A quantitative evaluation of the performance of the different registrations was necessary along with the visual ones. The mean diffusivity in the cortical regions of a cognitively normal individual ranges up to approximately $1.1 \cdot 10^{-3}$ mm^2/s [17]. Higher MD-values thus occur due to PVE from the CSF, which surrounds the cortex. Therefore the fraction of voxels with MD-values above $1.1 \cdot 10^{-3}$ mm^2/s was used as a PVE-index. Lower fractions would thus indicate a registration with higher accuracy due to less influence of PVE. The PVE-index was calculated by extracting the cortex from the MD-maps with a binary mask based on the T1-weighted image. The respective binary mask was available for all individuals after the preprocessing with FreeSurfer. Thereafter a segmentation of the MD-values was performed according to the above conditions, separating the high MD-values from the low ones. Lastly, a fraction was taken between the number of high MD-values and the total amount of MD-values in the cortex, which resulted in the PVE-indices. In some cases, the individual suffers from neurodegeneration which then changes the fraction since the mean diffusivity in the cortex changes with neurodegeneration.

The result was then displayed in a box and whiskers plot, showing the result between the different registrations by using different transformation methods but also the difference between using the b0 and the b2500 for driving the registrations. A comparison was also made between the 25 cognitively normal and the 25 individuals with mild cognitive impairment in another box and whiskers plot to see the differences. A paired t-test was then performed, comparing the means of respective registration for when the b0 and the b2500 were driving the registrations. Thereafter a two-way ANOVA without reproducability was performed as well both on the results from the b0 and the b2500 driving the registration. This would indicate if there was any significant difference between the different registrations using different transformations. The ANOVA tests were then followed by Tukey's post hoc honestly significant difference (HSD) tests. It tests the individual statistical significance between the different registrations using different transformations [28]. The HSD was calculated with the following equation

$$HSD = q\sqrt{\frac{MS}{n}}, \tag{3.1}$$

where q is the critical value which is extracted from a q-table [29]. The MS is the mean square error term from the ANOVA test and n is the size of the sample. After the calculation of the HSD, a mean of the respective registrations was taken. Thereafter all the means were subtracted from the means of the rest of the registrations driven by the same b-values image respectively. If the resulting difference between two different registrations were below the HSD-value, there would be a significant difference. All statistics were performed in Excel (Microsoft Corporation, Microsoft Excel, 2018).

3.5.4 PVE-indices across cortical regions

Besides only analyzing data in the cortex in general, an interesting aspect would also be to differentiate the cortical regions from one another and compare the performance of the registrations in the different regions. This was done with the Desikan–Killiany atlas, available in FreeSurfer which includes a segmentation of all the cortical regions in the brain. It was in a total of 70 regions including both the left and right hemispheres. The different cortical regions were evaluated by the PVE-indices as well. Before extracting the different cortical regions, a threshold was applied to the MD-maps which made it binary depending on which threshold was set. A threshold of $1.1 \cdot 10^{-3}$ mm^2/s was set, which would change all values below the threshold to zero and all above to 1 [17]. Thereafter a threshold making everything above $1.1 \cdot 10^{-3}$ mm^2/s to 0 and everything below into 1, was applied on the MD-images as well. This resulted in two different binary MD-maps, one containing the low MD-values and the other the high MD-values which normally do not belong in the cortex of a cognitively normal individual. Thereafter the Desikan–Killiany atlas was used to extract the cortical regions from both binary MD-maps. A PVE-index could then be calculated for the respective cortical region.

A density plot was created from the results of the extraction of the different cortical regions, both for the b0 and the b2500 driving the registrations for the different methods of registration. The average PVE-index between individuals for the respective cortical region was calculated. Thereafter the results were shown in a density plot, showing the distribution of the PVE-indices in the cortical regions for respective methods of registration. Three different cortical regions were chosen to be visualized separately as well in a box and whiskers plot, showing the PVE-indices for the different registrations. A safer region was chosen which was the inferior temporal lobe, where the occurrence of artifacts and disease is uncommon. A region where susceptibility artifacts in dMRI are common is the frontal lobe and more specifically the rostral middle frontal lobe. This region was therefore chosen as well. Lastly, a region where the presence of Alzheimer's is common in the early stages was also chosen and that is the entorhinal cortex [30].

3.5.5 Jaccard metric

A Jaccard similarity metric was also used to evaluate the differences between the images. An illustration of how the inputs for the calculation of the Jaccard index were produced is described below and can be observed in figure 3.4. An upper threshold was applied on the MD-maps resulting in them only including MD-values below $1.1 \cdot 10^{-3}$ mm^2/s i.e. The voxels that commonly belong to the cortex in a cognitively normal individual [17]. Thereafter the resulting image was made binary and the binary cortex mask from FreeSurfer was applied to it. This resulted in a binary mask of the cortex consisting of the voxels below $1.1 \cdot 10^{-3}$ mm^2/s. The binary cortex mask from FreeSurfer, which represents the cortex from the T1-weighted image, along with the binary cortex mask produced from the threshold was used as inputs for the calculation of the Jaccard index in equation 2.9. The Jaccard index was calculated for all individuals and respective methods of registration. Thereafter a box and whiskers plot was created to present the results.

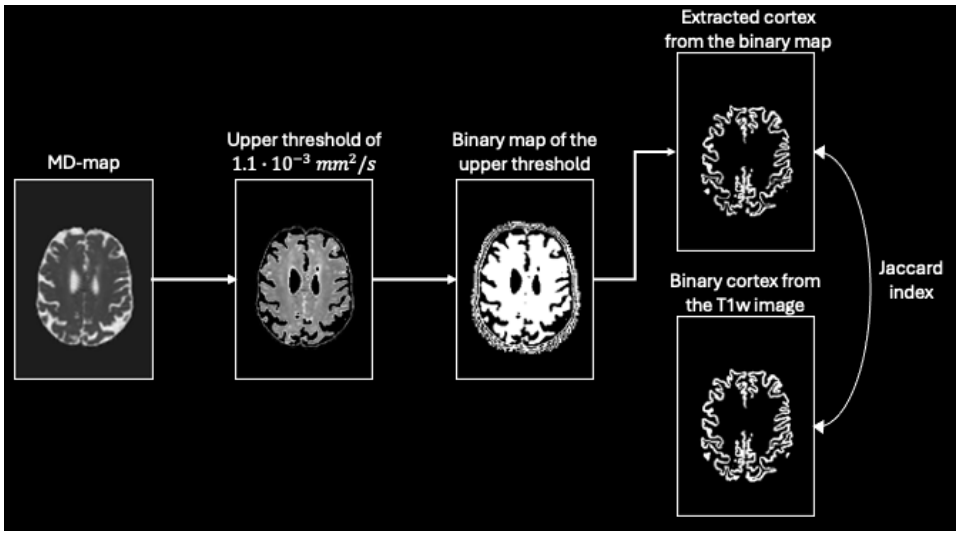

Figure 3.4: An illustration of the production of the inputs used for the calculation of the Jaccard index. From the left, it starts with an extraction of the low MD-values from the MD-map which is then made binary. Thereafter the cortex was extracted from the binary map with the cortex mask from FreeSurfer. To the right in the figure, the inputs for the calculation of the Jaccard index can be seen to be the binary cortex map after applying the threshold and the binary cortex map from FreeSurfer.

3.6 Bowsher priors

After the registrations were performed, a reconstruction algorithm, the Bowsher prior that increases the resolution of the images, was applied to the registered DWIs. The implementation of the reconstruction algorithm was based on the steps outlined in an article [24]. After the images were reconstructed the MD-maps were calculated with the use of equation 2.1. After that, an evaluation of the reconstructed images was performed by comparing them to the registered diffusion-weighted images that were not reconstructed.

4 Results

4.1 Visual evaluation

The visual evaluation showed a clear difference between the different registrations which can be observed in figure 4.1 and 4.2. It was also clear from the beginning that none of the registered diffusion images seemed to be perfectly aligned with the T1-weighted image. The outlining of the cortex of the combined method used for the registrations seems to be deviating the most, both for the b0 and the b2500 driving the registrations. The tissue appears to have shrunk in comparison to the T1-weighted image in figure 4.1 and 4.2. In the central anterior part, a large deviation can also be observed where the tissue in the combined looks more blurred in comparison to the other registrations. The other registrations including rigid, affine and nonlinear behave more similarly to one another in figure 4.1. A slight deviation can be observed in the anterior part between them. The affine seems to have similar tendencies as the combined regarding the shrinking of the tissue, however not quite as dramatic. The same goes for the nonlinear registration method in some areas. The rigid looks however to be contained within the mask and presents with the most similarities to the T1-weighted image in this case.

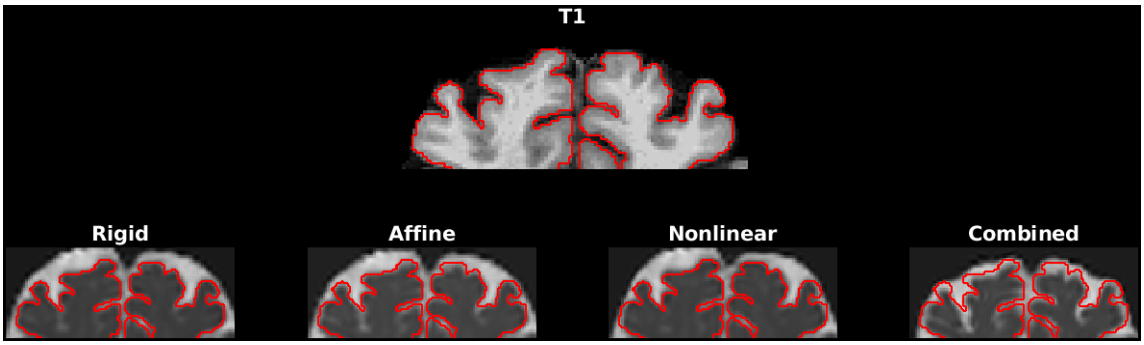

Figure 4.1: The outlining of the T1-weighted image in the anterior part of the brain, together with the four registration approaches (driven by b0) used where the outlined mask is applied on the MD-image.

When the b2500 is driving the registrations instead, the rigid, affine and nonlinear become more visually similar to one another which can be seen in figure 4.2. The outlining seems to have a better fit, and a higher similarity regarding the location of the cortex can be observed in figure 4.2 in comparison to figure 4.1. The b2500 driving the registration seems to have some benefits in comparison to when the b0 is driving the registrations.

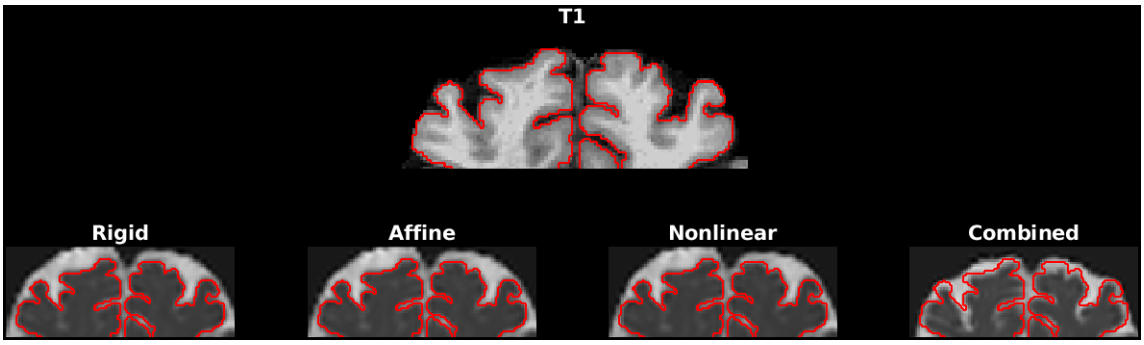

Figure 4.2: The outlining of the T1-weighted image in the anterior part of the brain, together with the four registration approaches (driven by b2500) used where the outlined mask is applied on the MD-image.

This method of visual evaluation is useful for a quick evaluation of the registration. However it proves to be more useful if a slice where the registration accuracy decreases has been identified in advance, an example of this can be seen in figure 4.3. This visual evaluation method can be used for differentiating registrations from one another however conclusions about the performance of the registrations can not be drawn by using this method. This is because this method is dependent on which slice is being observed. The nonlinear seemed to give a high registration accuracy in figure 4.1 and 4.2, however in a different slice the accuracy of the registration decreased by a lot which can be seen in figure 4.3. This unpredictable behavior of the registrations can go undetected in this visual evaluation.

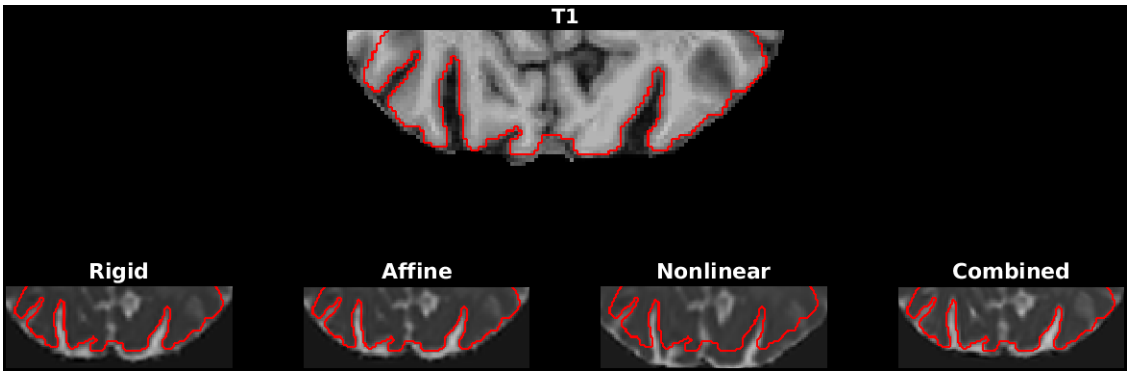

Figure 4.3: The outlining of the T1-weighted image in the posterior part of the brain, together with the four registration approaches (driven by b0) used where the outlining is applied on the MD-image. The outlining of the nonlinear is not located around the cortex as it should be, implying a low registration accuracy. The Jaccard indices for the registrations are the following from left to right: 0.9822, 0.9767, 0.9809, 0.9586.

Accordingly, this method has limitations due to the outlining of the nonlinear appearing to be accurate in figure 4.2 but proved otherwise in figure 4.3. This method could thus be more helpful in finding errors in the registrations rather than proving that the registrations have a high accuracy.

4.2 Difference maps

The difference maps, created by taking the difference between the DWI and the T1-weighted image after the intensity scaling, can be used to visualize the performance of the different registrations similar to the method before with the outlining of the cortex. It can be seen in figure 4.4 that the combined method shows the highest intensity and contrast in the image, meaning that this method of registration gave the lowest accuracy. The intensity of the rigid, affine and nonlinear are less expressed in comparison to the combined. There are nevertheless some differences between them, for instance, the overall impression shows that the intensity of the rigid seems to be slightly higher than for the affine and nonlinear. The registrations with the nonlinear and affine transforms can however barely be differentiated in this scenario.

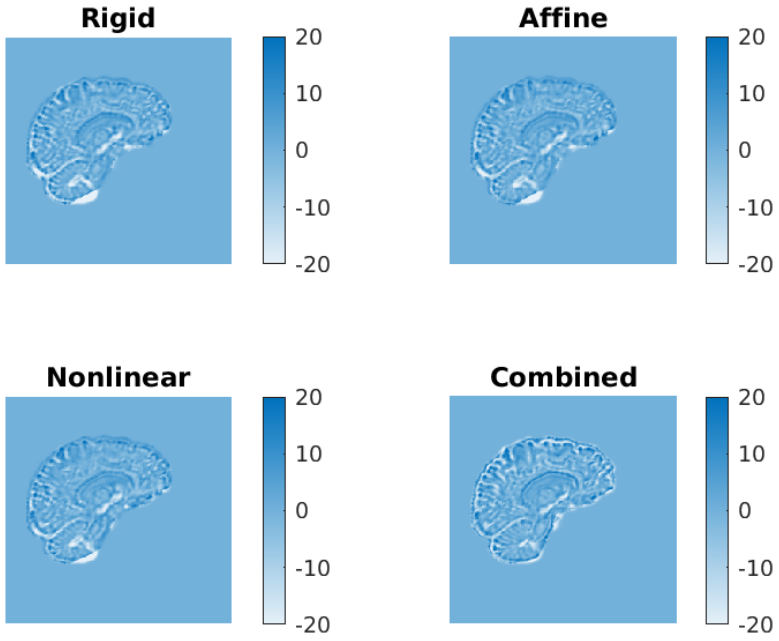

Figure 4.4: The difference maps between the registered DWIs and T1-weighted image created after the intensities in the DWIs had been scaled to be similar to the ones in the T1-weighted image. A high intensity represents a larger difference between the images.

This method visualizing the differences between the registered DWIs and the T1-weighted image highlights regions where the registration accuracy appeared to be low. This method is however also only used for one slice, which implies a slice dependence in this case as well. Hence this method would also be more helpful in finding regions of low registration accuracy rather than proving that the registration in general has a high accuracy.

4.3 PVE-indices in the cortex

The PVE-index comes from the segmentation of the MD-values in the cortex and it can be seen in figure 4.5 that the PVE-indices differ between the different registrations both for the b0 (left) and the b2500 (right) driving the registrations. A lower PVE-index indicates a more accurate registration with less influence of PVE from the CSF. The registration performed with a combined method presents with the highest PVE-indices both for when the b0 and the b2500 are driving the registrations which can be seen in figure 4.5. When the b0 is used to drive the registration, rigid has the lowest median and spread of data. This result thus indicates that it performed the best for the b0 driving the registrations. The nonlinear has a slightly higher median and contains outliers of higher PVE-indices. The affine can be seen to not perform sufficiently in comparison to the rigid and the nonlinear one. The two-way ANOVA without reproducibility showed a statistically significant difference between registrations when the b0 was driving the registrations. Tukey's post hoc HSD test then revealed a significant difference between all four registrations.

In figure 4.5 for the b2500 driving the registration the results between rigid, affine and nonlinear are more similar which could be suggested already in the outlined figure 4.2. The median is very similar between the affine and the nonlinear registrations whereas the median for rigid is just slightly higher. The combined is however still deviating a lot from the others in this case as well. The spread of the rigid, affine and nonlinear registration are similar as well, suggesting that the results indicate a similar performance between the three transforms used in the registrations. The two-way ANOVA without reproducibility showed a statistically significant difference between registrations when the b2500 was used. Tukey's post hoc HSD test then revealed a significant difference between all registrations except the rigid and affine as well as between the affine and the nonlinear.

The difference between the b0 and the b2500 driving the registration can also be observed in figure 4.5. Affine seems to be impacted a lot by whether the b0 or the b2500 is driving the registration. Rigid however seems to be performing more consistently independent of if the registration is driven by a low or high b-value image. The nonlinear can also be seen to have some dependence on this since the outliers present when the b0 was driving the registration, are gone when the b2500 is used. A statistically significant difference was revealed with paired t-tests for all registrations ($p < 10^{-6}$) indicating that the registration accuracy was better when the b2500 was driving the registrations.

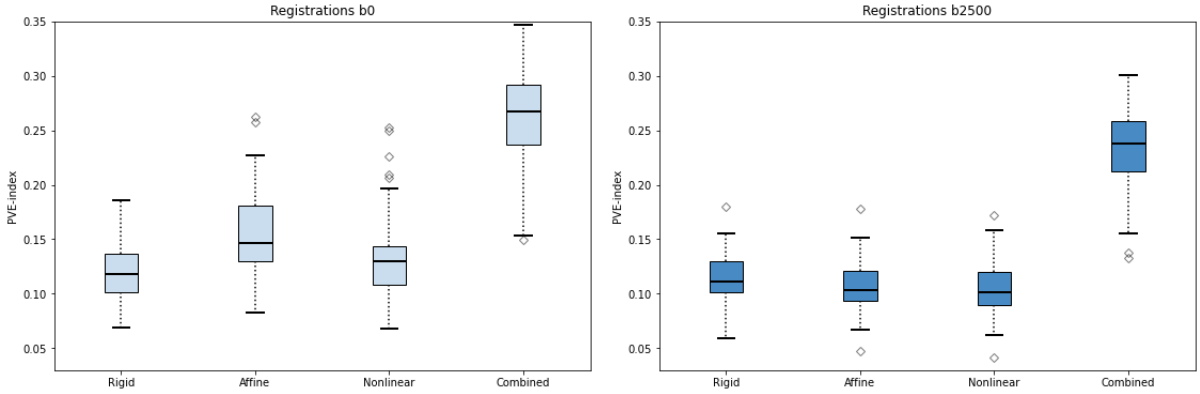

Figure 4.5: The performance of the four different methods used for registration, measured in a PVE-index in the cortex. The figure to the left is driven by the b0 and the figure to the right is driven by the b2500.

Moreover, a difference between the registrations for the cn and mci individuals can be observed in figure 4.6 for both the b0 and the b2500 driving the registrations. The cn population consisting of 25 individuals was in all cases presenting with a lower PVE-index than the mci. The changes in the brain during Alzheimer's disease modify the morphology of the brain. Due to this, the registrations have a harder time aligning the images to one another. Thus it will be easier for the registrations to align a healthy brain in comparison to a brain that has started to undergo complex changes. Due to the investigation regarding finding AD in an early stage, it would be preferred if the registrations had higher accuracy in the cases of individuals with mci. No extensive biases can be observed in figure 4.6 between the cn and the mci for any method of registration in the b0 nor the b2500 driving the registrations.

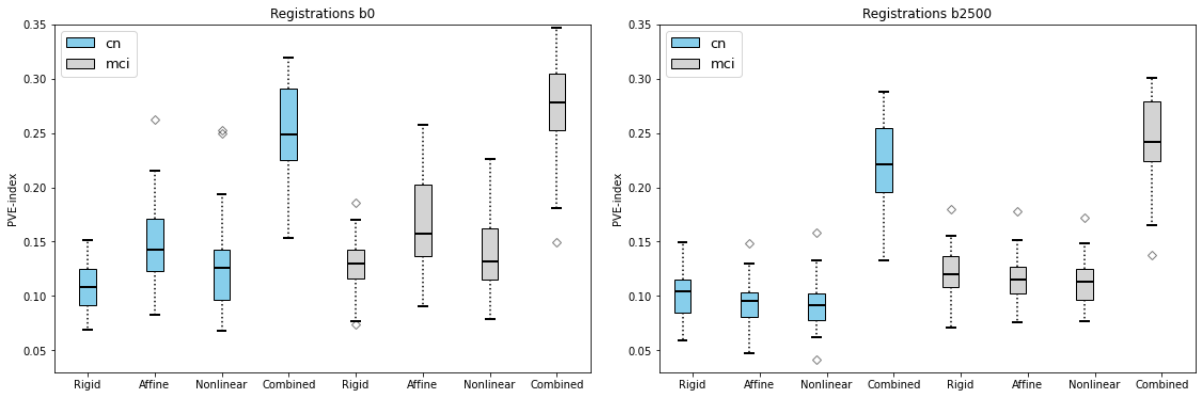

Figure 4.6: The different registration performance depends on whether the individual had mci or cn. The left figure shows the results from when the b0 is used for the registrations and the figure to the right is when b2500 is used.

4.4 PVE-indices across cortical regions

The density plots were created by averaging the PVE-indices for respective cortical regions between individuals for the different registrations. The result can be observed in figure 4.7.

The results from the 50 individuals show again that there is a difference between the b0 and the b2500 driving the registrations. It also implies that there is a difference in performance between the registrations regarding the different cortical regions. In some cortical regions, the average PVE-indices are relatively small in comparison to other areas where the registrations had a lower accuracy, which for instance could be in regions where artifacts are more common.

In the case when the registrations are driven by the b0, the distributions of the PVE-indices can be distinguished between the different methods of performing the registrations, which can be seen in figure 4.7. The combined method has a wide spread and both the affine and nonlinear transforms present with a tail in the distribution. The center of the distribution for the registrations using rigid, affine and nonlinear transforms are however similar. The rigid did however perform the best in this case.

The distributions of the rigid, affine and nonlinear are more similar when the b2500 is driving the registrations which can be seen in figure 4.7. The distribution of the affine and nonlinear becomes more narrow in comparison to when the b0 was used. The shape of the combined registration however remains approximately the same.

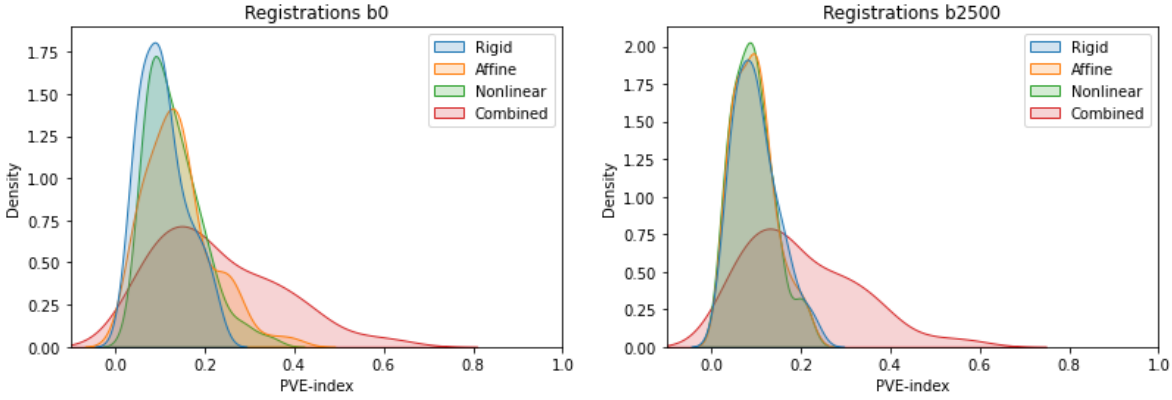

Figure 4.7: Density plots of the 70 different cortical regions averaged over individuals for different registrations. The left figure shows the results from when the b0 is driving the registrations and the right shows the results of when the b2500 is driving the registrations.

Box and whisker plots were created for three different regions of the cortex for a more thorough investigation of how the registrations performed in different regions. The regions chosen were a simple region (expected to be without artifacts and signs of disease), a region affected by artifacts, and a region where Alzheimer's disease is likely to be present in an early stage. The results from the three regions can be seen in the figures 4.8, 4.9 & 4.10.

The results for the simple region, which is the inferior temporal cortex in figure 4.8, shows that the PVE-indices are low in comparison to what has been observed before, for instance in figure 4.5 above. The results between the b0 and the b2500 driving the registrations are relatively similar as well, where larger deviations have been observed before, for instance in figure 4.5. There is a clear difference between the results from the cn and mci where the PVE-indices for the mci tends to be larger overall. The registrations thus seem to be performing better in a less complex region which most commonly is not affected by artifacts and disease.

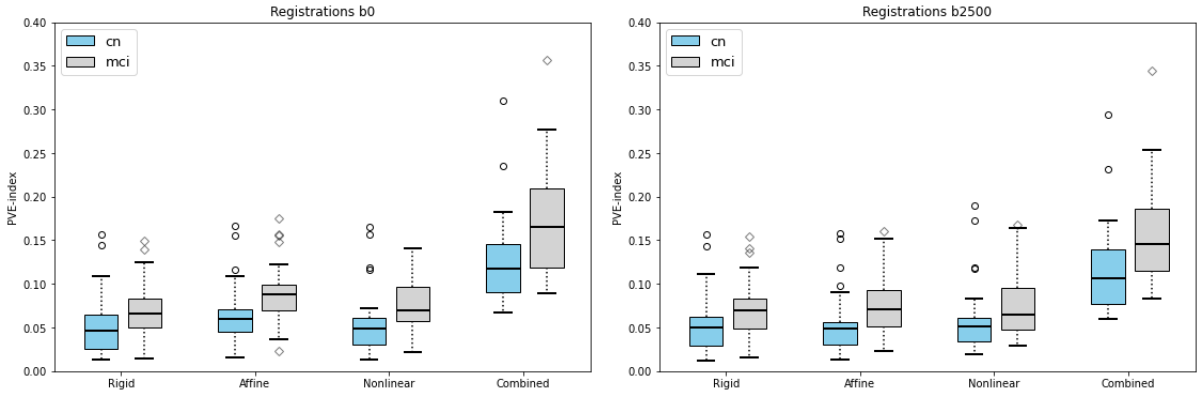

Figure 4.8: The performance of the different registrations in the inferior temporal cortex, which usually is a simple region without any artifacts and signs of disease. The results separate the individuals with conditions that are either cn or mci and in the figure to the left the b0 drives the registrations and to the right, the b2500 drives the registrations.

For a region where artifacts are more common, such as in the rostral middle frontal cortex, the results are expected to have higher PVE-indices which can be confirmed by the result in figure 4.9. The correction for susceptibility artifacts is rarely entirely successful, thus resulting in residue from the artifacts and changes in the anatomy in the DWI. Consequently, the PVE-indices in this region are relatively higher than what they have commonly been seen to be before in for instance figure 4.5. The combine presents with the highest PVE-indices thereby indicating that it has the lowest registration accuracy. The results from the registrations using affine and nonlinear transforms differ vastly depending on whether the b0 or the b2500 is driving the registration. Hence by using the b2500 to drive the registrations, the PVE-indices can be decreased substantially for the affine and nonlinear. The rigid however proves to be robust to whether the b0 or b2500 is driving the registrations with only a slight difference in PVE-index.

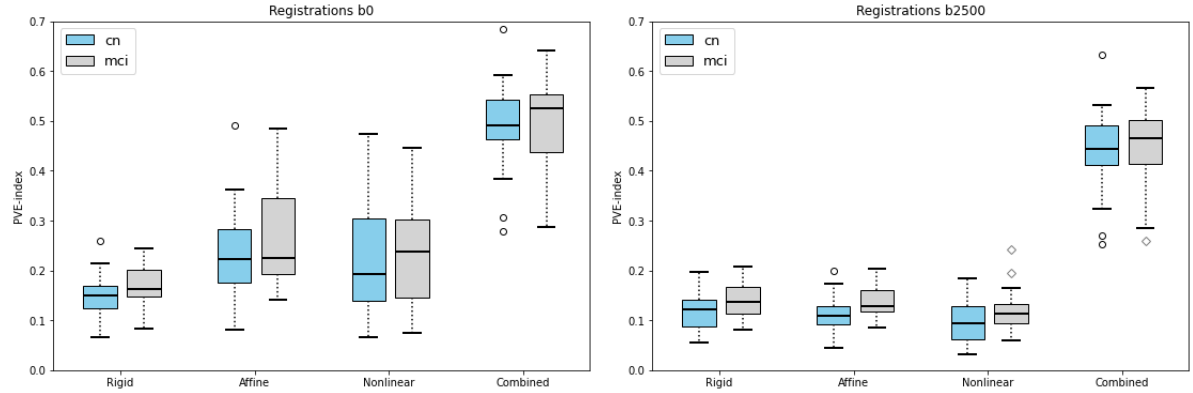

Figure 4.9: The performance of the different registrations in the rostral middle frontal cortex where artifacts usually are common. The results separate the individuals with cn respectively mci, and in the figure to the left the b0 drives the registrations and to the right, the b2500 drives the registrations.

The results of the PVE-indices in a cortical region where Alzheimer's disease commonly appears in an early stage can be seen in figure 4.10, where the cortical region is called the entorhinal cortex. This is the first result where the combined method does not deviate from the other methods of registration but instead has a similar performance to them. The combined does not seem to be very affected by which b-value drives the registrations either which it has in common with the rigid in this case. The affine and nonlinear perform better when the b2500 is driving the registration again. The decrease of the nonlinear (cn) from when the b0 was driving the registrations to when b2500 is however huge. A concern about this result is that it could

be misleading due to the PVE-index being that low. An unintentional inclusion of white matter in the mask of the entorhinal cortex could have happened, causing the registration accuracy to look great when it is not.

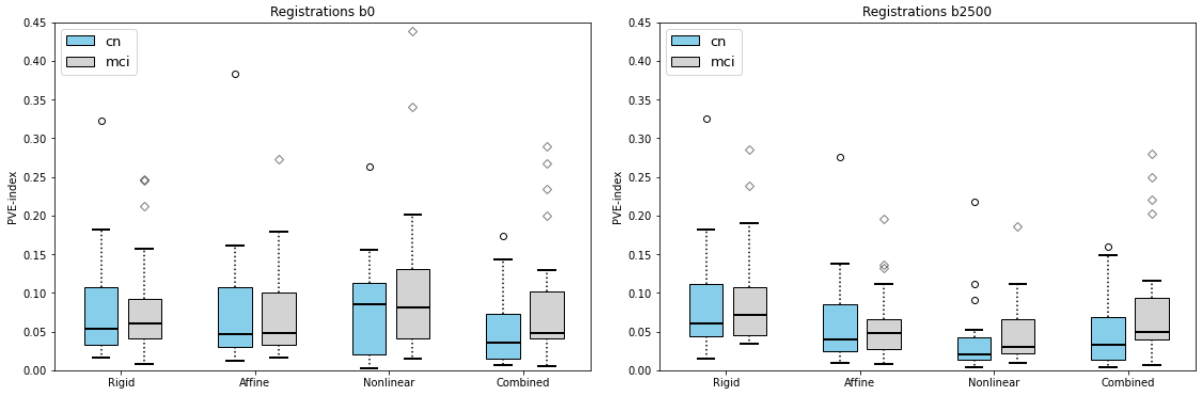

Figure 4.10: The performance of the different registrations in the entorhinal cortex where the first signs of Alzheimer's disease usually are present. The results separate the individuals with cn from the individuals with mci and in the figure to the left the b0 drives the registrations and to the right, the b2500 drives the registrations.

4.5 Jaccard metric

The Jaccard metric was calculated from the binary segmentation of the voxels in the cortex with a mean diffusivity below $1.1 \cdot 10^{-3}$ mm^2/s and the binary cortex mask of the T1-weighted image. The results can be observed in figure 4.11.

A Jaccard Index of 1 implies an exact match between the objects that are being compared and in figure 4.11 it can be seen that the registrations are overall resulting in high Jaccard indices. There are also some differences between the b0 and the b2500 driving the registrations. The overall results have similar behavior to the results in figure 4.5 but are shown and calculated in different ways. Both ways are still necessary and useful to present, since in figure 4.11 the similarity of the cortices between the registered diffusion images and the T1-weighted image is shown. Nevertheless, it can be observed that when the b2500 drives the registrations, a higher Jaccard index is achieved which corresponds to the results above in figure 4.5 as well.

The results indicate that the combined method used to perform the registrations generates a cortex with the lowest similarity to the cortex in the T1-weighted image which can be seen in figure 4.11. For the b0 driving the registrations, the rigid seems to be resulting in the highest similarity and for the b2500 the nonlinear has the highest similarity. The rigid however also present with a high similarity when the b2500 is driving the registration and the results indicate robustness when rigid is used, which has been seen in figure 4.5 as well.

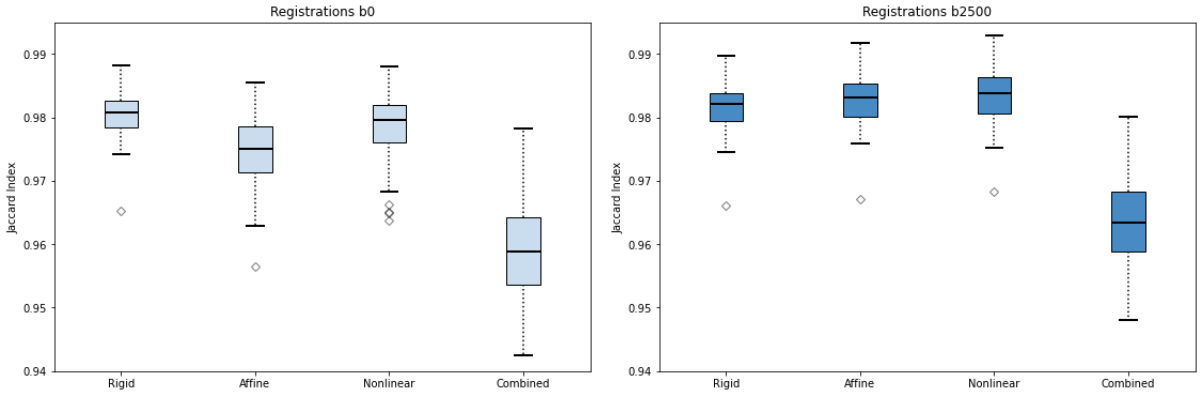

Figure 4.11: The Jaccard indices of the b0 (left) and the b2500 (right) driving the registrations along with the four different methods used for the registrations.

4.6 Bowsher priors

To further increase the resolution of the diffusion-weighted image, in an attempt to achieve less partial volume effects, Bowsher priors were used. The Bowsher prior method performs a reconstruction of the registered DWI with the T1-weighed image as an input to increase the resolution of the DWI.

The result of the reconstructed diffusion-weighted image with the Bowsher prior method can be observed in figure 4.12. A difference between the Bowsher prior image and the so-called regular DWI (registered DWI without a Bowsher prior method applied) can be seen visually where the reconstructed image has a higher resolution. To the right in figure 4.12 a subtraction between the Bowsher and the regular DWI has been taken which shows the difference between them. It seems like the difference exists mainly in the edges and the small structures and ventricles of the brain. Since the cortex is located in the peripheral parts of the brain, it can be expected that there will be a difference between cortical evaluations of the Bowsher and the regular DWI.

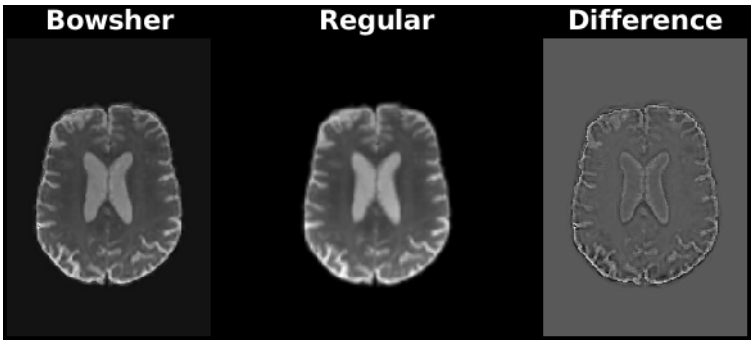

Figure 4.12: The result of the reconstruction of the DWI with the Bowsher prior to the left, the regular registered DWI before reconstruction in the center, and the difference between the images to the right.

A mean diffusivity map was calculated from the Bowsher prior reconstructed DWI. In figure 4.13 the MD-maps of a random slice of the Bowsher prior and the regular DWI can be observed. It is noticeable that the intensities of the images are different and that can be observed in the difference images as well to the right in figure 4.13. From the difference image, where the regular diffusion image has been subtracted from the Bowsher prior image, it can be seen that the MD values are higher in the Bowsher prior image in the entire slice. The intensity is especially high in the peripheral regions of the brain, i.e. Where the cortex is. This

result implies that the Bowsher prior reconstruction method changes the values of the diffusion image which makes the MD-values not credible.

Consequently, the results will not be presented with PVE-indices like the rest of the results since the Bowsher prior reconstruction algorithm changes the values extensively in the DWI. From figure 4.13 it can already be seen in the difference image that the MD-values are higher in the cortex and therefore will result in higher PVE-indices as well. The Bowsher prior reconstruction algorithm thus needs to be further optimized to be compared and evaluated by the PVE-indices in the cortex.

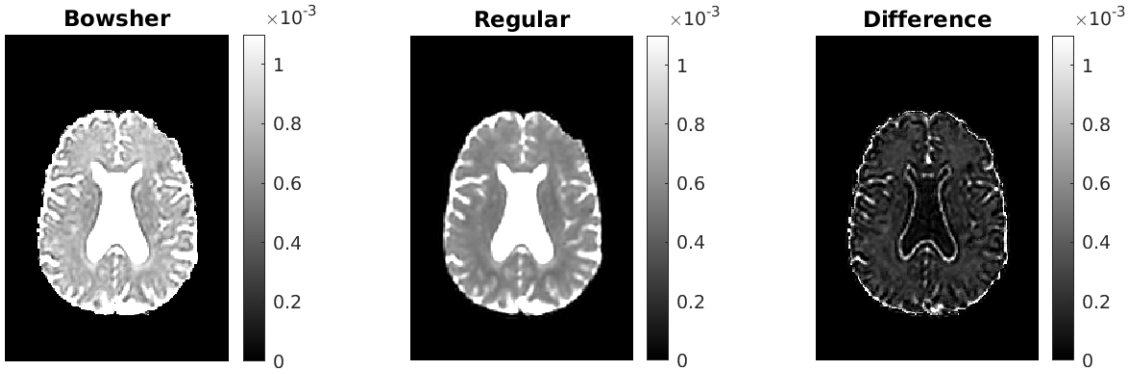

Figure 4.13: MD-maps of a slice in a Bowsher prior reconstructed DWI along with the regular DWI before the reconstruction. Furthest to the right, a difference image can be seen which shows the subtraction of the Regular from Bowsher.

5 Discussion

The intent of this work was to investigate different ways of performing a registration to find the most accurate one. The results suggest that the combined performed the worst out of the different methods used for performing a registration that was investigated. The results also indicated that the most accurate registration occurred when the b2500 was driving the registrations. Furthermore, the rigid, affine and nonlinear transformations performed with the highest registration accuracies when the b2500 was used.

The results based on the 50 individuals including 25 cognitively normal individuals and 25 mildly cognitive impaired individuals, indicated that using the b2500 to drive the registration was superior to using the b0. The PVE-indices decrease which can be observed in figures 4.5-4.10. The paired t-tests confirmed a significant difference ($p < 10^{-6}$) between registrations driven by b0 or b2500. The PVE-indices were however only evaluated in the cortex, thus restricting these results to the registration accuracy in the cortical regions. A study has shown that registrations are more consistent and contain less variability when the moving image $I_m(x)$ has a similar contrast to the reference image $I_r(x)$ [22]. The contrast of the b2500 is similar to the contrast of the T1-weighted image whereby the contrast from the b0 is however more different due to the high signal from the CSF for instance. The results regarding the b2500 having a higher registration accuracy can thus be supported by that study [22]. A higher b-value implies a higher diffusion weighting, meaning that areas containing a high diffusivity will generate a low signal. The signal from the CSF will thus be suppressed due to the high diffusivity in the fluid, resulting in an image with sharper lines in for instance the peripheral parts of the brain where the cortex is located. The sharper lines can be an advantage during the registration process, making the alignment easier. In summary, the results indicate that the registrations should be driven by a b2500 image or a higher b-value image which has a more similar contrast to the T1-weighted image to result in a better registration, at least for the cortical regions.

The performance of the registration is also dependent on how the registration is implemented regarding which transforms that is used for instance. The different methods of how the registration is performed have in turn a dependence on which b-value that is used to drive the registrations. When the b0 is driving the

registration, some of the results above suggest that the rigid performs the best with the smallest PVE-index which can be seen in for instance figures 4.6 & 4.7. The nonlinear has a similar performance to the rigid in many cases where the medians seem to be approximately the same which can be seen in figures 4.5 & 4.11 for instance. The whiskers belonging to the registration when the nonlinear transform is used seem however to be longer and contain more outliers indicating that the data has a wider distribution than what it has for rigid. Tukey's post hoc HSD test confirmed a statistical difference between the rigid and the nonlinear when the b0 was driving the registration, indicating that the rigid had a higher registration accuracy in this case. When the b2500 was driving the registrations the results were more difficult to differentiate between the rigid, affine and nonlinear. The median of the affine and nonlinear are similar in most cases which can be seen in for instance figures 4.5 & 4.11. The Tukey's post hoc test revealed that there was no statistically significant difference between them. Furthermore, it also showed no significant difference between the rigid and the affine either. However, there was a significant difference between the rigid and nonlinear although the rigid, affine and nonlinear seemed to be distributed similarly in for instance figure 4.5. Generally, there is no consensus in studies regarding which method for registration which is superior to use. Most studies use different ways to perform registrations, with different software, transforms and other implementations of the registrations [10–12]. The result from this work suggests that it could be because most registrations generate a similar registration accuracy. That was the case for registrations using the transforms rigid, affine and nonlinear when the b2500 was driving the registrations in this work. Therefore a single method of performing a registration with the highest accuracy cannot be stated at this time. This is due to the different registrations converging towards the best registration accuracy together in the current resolution.

The evaluation methods used in this work could be used for differentiation between registration accuracies. The results from the evaluation methods implied which registrations produced the highest accuracy when the b0 and the b2500 were driving the registrations, as well as indicating a superior registration accuracy when the b2500 was used. In the case of when the b2500 was driving the registrations the result with the evaluation method regarding the PVE-indices implied that the rigid, affine and nonlinear transforms generated results with a similar registration accuracy. This suggests that these transforms could be interchangeable during registrations, using the b2500 as a moving image, depending on which purpose the user has for the registration or what the data looks like. For instance, if the data suffers from strong susceptibility artifacts, a nonlinear transform would be more useful for the registration to alleviate the artifacts instead of using a rigid one. The visual evaluations used in this work could however also be used to indicate a difference between the registrations. However, the assessment can not be as thorough in a visual evaluation as in a computed one. Nevertheless, in some studies, a visual evaluation might be sufficient as an evaluation method [11, 12]. It depends on the purpose of the study as well as to what extent the results are going to be used. A qualitative way of evaluating the registrations is however dependent on the individual evaluating the images. However, in this work regarding the mapping of microstructures, a higher accuracy of the registrations becomes more relevant which calls for a need to have a computed method of evaluation. Therefore the visual evaluation which can be seen in figures 4.1, 4.2 & 4.4 are not enough to determine the accuracy of a registration in this work. Although the PVE-indices were a simple evaluation method, it was useful for the differentiation of the results when a quantitative evaluation is necessary. However, it can be seen in figure 4.3 that the registrations performed with a nonlinear transform can result in a registration with low accuracy in some regions. This behaviour is not reflected in the PVE-indices, since the MD-values will be lower than what they are when the CSF is included in them. The PVE-indices could therefore indicate a result with a decreased amount of PVE, although the accuracy of the registration was not sufficient. Thus the PVE-indices is a metric with limitations regarding the indication of whether the registrations were successful or not.

The need for decreasing the partial volume effects however remains. A study shows that there is an important need to correct for partial volume effects further in the investigation of the MD in cortical regions in Alzheimer's disease [10]. This is because the morphology of the cortex changes due to AD, thus implying that it is more affected by PVE which can be suggested in figure 4.6. By performing corrections of the PVE the results can perhaps lead to an improvement in methods to distinguish changes in MD-values in the cortical regions. Partial volume effect can also be decreased after the registrations with the use of a Bowsher prior method [24]. The Bowsher priors could be used to increase the resolution in the registered DWI. The results from the Bowsher prior algorithm indicated that the resolution was increased which can be confirmed by figure 4.12. However, according to the MD-maps on which the evaluations of the PVE-indices

were based on, the reconstruction changed the values of the DWI which can be seen in figure 4.13. Due to that, this method could not currently be evaluated and used for a comparison with the registered DWI (regular DWI) before the Bowsher prior was applied. It would have been interesting to see if the Bowsher priors could have been used in gathering more information about the difference in performance of the rigid, affine and nonlinear transforms used when the b2500 was driving the registration. It would also have been interesting to see the results regarding how the Bowsher priors would have handled a region such as the rostral middle frontal cortex which suffers from susceptibility artifacts, which can be seen in figure 4.9. The Bowsher algorithm however needs some optimization before any conclusions can be drawn about whether this method can decrease the influence of the partial volume effects further.

There are a few limitations in this work. The first one was that only one software was used to run the registrations and that was ANTs. By including other software as well, the results might suggest other conclusions than the current ones. From the neuroimaging perspective, and especially the mapping of microstructures, it would have been beneficial to determine the best software for the respective registration method as well. The PVE-indices used for the evaluations were limited to comparing the registration accuracy in the cortex and not the entire brain volume. However, in this work, those were the regions of interest. An additional limitation of the PVE-indices was that there was no certainty that the white matter accidentally contributed to the PVE-index. In figure 4.3 the nonlinear transform can be seen to expand the brain volume. In that case, the cortical mask applied would also include MD-values from the white matter which would affect the PVE-indices. This behavior has however for the most part been seen in the registrations driven by the b0.

6 Conclusion

The results suggest that the rigid transform produced the highest registration quality when the b0 was driving the registrations. This was seen in the visual evaluations as well as the evaluations with the PVE-indices. The affine, nonlinear and combined had more outliers indicating that the registrations performed with them had a lower quality in some cases, which could be seen in the evaluation with the PVE-indices. When the b2500 was used to drive the registrations, the registration quality increased and became similar for rigid, affine and nonlinear. This could be seen in the visual evaluations as well as the evaluations with the PVE-indices. This indicates that the transforms used for the registrations could be interchangeable when using b2500 data. Lastly, the results suggest that the analysis of registration accuracy is not straightforward.

7 Future prospects

The registration accuracy has been investigated before, in many different ways, but the need remains [12, 22, 31]. Other evaluation techniques are needed to more accurately evaluate the entire brain volume and not only the cortical areas. The results suggested that combined did not perform with a high registration quality. However, it cannot be excluded before it has been investigated further with for instance the multimodal registration framework (MMORF) from FSL which is another way of performing a registration with a combined method [32]. Other software needs to be investigated and better tools for analyzing registration accuracy. Especially in the context of mapping cortical microstructures with dMRI.

Acknowledgements

First and foremost I would like to express my gratitude towards my amazing supervisors.

> **Markus Nilsson & Nicola Spotorno,** thank you for your expertise and creative ideas during this work. Your inputs has been invaluable as well as your support and guidance this semester. I have learned a lot from you both that I will take with me for the future.

For my office neighbors, thank you for your encouragement and the recognition you have given me during this semester. Our discussions have been both fun and valuable to me.

A special thanks to my wonderful classmates who have made the last couple of years studying even better than I could imagine. Our weekly catch-ups during this semester have given me energy and encouraged me to continue the hard work. It has been a pleasure to have you as classmates.

Lastly, to my friends and family, thank you for the endless support you have given me, not only during this semester but also during the 5 years that led up to this moment. Thank you for always being there for me.

References

[1] Soria Lopez JA, González HM, and Léger GC. Chapter 13 - Alzheimer's disease. Handbook of Clinical Neurology. Vol. 167. Geriatric Neurology. Elsevier. Jan 2019. URL: https://www.sciencedirect.com/science/article/pii/B9780128047668000133.

[2] Hansson O. Biomarkers for neurodegenerative diseases. Nat Med 27, 954–963. ISSN: 1546-170X. June 2021. URL: https://www.nature.com/articles/s41591-021-01382-x.

[3] Alzheimer's Disease Fact Sheet. National Institute on Aging (NIA), Reviewed: April 2023. URL: https://www.nia.nih.gov/health/alzheimers-and-dementia/alzheimers-disease-fact-sheet.

[4] Vogt NM, Hunt JF, Adluru N, Dean DC, et al. Cortical Microstructural Alterations in Mild Cognitive Impairment and Alzheimer's Disease Dementia. Cereb Cortex. 2020 May 14;30(5):2948-2960. doi: 10.1093/cercor/bhz286. PMID: 31833550; PMCID: PMC7197091. URL: https://www.ncbi.nlm.nih.gov/pmc/articles/PMC7197091/.

[5] Le Bihan D. Diffusion MRI: what water tells us about the brain. EMBO Molecular Medicine 6.5. ISSN: 1757-4676. Num Pages: 573 Publisher: Springer Nature. May 2014. URL: https://www.embopress.org/doi/full/10.1002/emmm.201404055.

[6] Eustache P, Nemmi F, Saint-Aubert L, Pariente J and Péran P. Multimodal Magnetic Resonance Imaging in Alzheimer's Disease Patients at Prodromal Stage. Journal of Alzheimer's Disease. Vol. 50. ISSN: 1387-2877. Jan. 2016. URL: https://www.ncbi.nlm.nih.gov/pmc/articles/PMC4927932/.

[7] Spotorno N, Strandberg O, Vis G, Stomrud E, Nilsson M and Hansson O. Measures of cortical microstructure are linked to amyloid pathology in Alzheimer's disease. Brain. 2023 Apr 19;146(4):1602-1614. doi: 10.1093/brain/awac343. PMID: 36130332; PMCID: PMC10115177. URL: https://www.ncbi.nlm.nih.gov/pmc/articles/PMC10115177/.

[8] Fischl B and Dale AM. Measuring the thickness of the human cerebral cortex from magnetic resonance images. Proc Natl Acad Sci U S A. 2000 Sep 26;97(20):11050-5. doi: 10.1073/pnas.200033797. PMID: 10984517; PMCID: PMC27146. URL: https://www.ncbi.nlm.nih.gov/pmc/articles/PMC27146/.

[9] McHugh TL, Saykin AJ, Wishart HA, Flashman LA, et al. Hippocampal volume and shape analysis in an older adult population. Clin Neuropsychol. 2007 Jan;21(1):130-45. doi: 10.1080/13854040601064534. PMID: 17366281; PMCID: PMC3482482. URL: https://www.ncbi.nlm.nih.gov/pmc/articles/PMC3482482/.

[10] Henf J, Grothe MJ, Brueggen K, Teipel S and Dyrba M. Mean diffusivity in cortical gray matter in Alzheimer's disease: The importance of partial volume correction. Neuroimage Clin. 2017 Oct 4;17:579-586. doi: 10.1016/j.nicl.2017.10.005. PMID: 29201644; PMCID: PMC5702878. URL: https://www.ncbi.nlm.nih.gov/pmc/articles/PMC5702878/.

[11] Bhushan C, Haldar Justin P, Choi S, et al. Co-registration and distortion correction of diffusion and anatomical images based on inverse contrast normalization. Neuroimage Vol. 115. ISSN: 1053-8119. July 2015. URL: https://www.sciencedirect.com/science/article/pii/S1053811915002451.

[12] Visser M, Petr J, Müller DMJ, Eijgelaar RS, et al. Accurate MR Image Registration to Anatomical Reference Space for Diffuse Glioma. Front Neurosci. 2020 Jun 5;14:585. doi: 10.3389/fnins.2020.00585. PMID: 32581699; PMCID: PMC7290158. URL: https://www.ncbi.nlm.nih.gov/pmc/articles/PMC7290158/.

[13] Mori S and Barker PB. Diffusion magnetic resonance imaging: Its principle and applications. The Anatomical Record. Vol. 257. ISSN: 1097-0185. 1999. URL: https://onlinelibrary.wiley.com/doi/abs/10.1002/%28SICI%291097-0185%2819990615%29257%3A3%3C102%3A%3AAID-AR7%3E3.0.CO%3B2-6.

[14] O'Donnell LJ and Westin CF. An introduction to diffusion tensor image analysis. Neurosurg Clin N Am. 2011 Apr;22(2):185-96, viii. doi: 10.1016/j.nec.2010.12.004. PMID: 21435570; PMCID: PMC3163395. URL: https://www.ncbi.nlm.nih.gov/pmc/articles/PMC3163395/.

[15] Forseen SE, Gilbert BC, and Figueroa RE. Chapter 2 - Imaging of glioblastoma recurrence. New Targeting in the Reversal of Resistant Glioblastomas. Vol. 14. Academic Press. Jan. 2021. URL: https://www.sciencedirect.com/science/article/pii/B9780128225271000034.

[16] Spotorno N, Strandberg O, Stomrud E, Janelidze S, et al. Diffusion MRI tracks cortical microstructural changes during the early stages of Alzheimer's disease. Brain. Vol. 147. ISSN: 0006-8950. Mar. 2024. URL: https://doi.org/10.1093/brain/awad428.

[17] Elman JA, Panizzon MS, Hagler DJ, Fennema-Notestine C, et al. Genetic and environmental influences on cortical mean diffusivity. Neuroimage. Vol. 146. ISSN: 1053-8119. Feb. 2017. URL: https://www.sciencedirect.com/science/article/pii/S1053811916306474.

[18] Van Reeth E, Tham IWK, Tan CH and Poh CL. Super-resolution in magnetic resonance imaging: A review. Concepts in Magnetic Resonance Part A. Vol. 40A. ISSN: 1552-5023. 2012. URL: https://onlinelibrary.wiley.com/doi/abs/10.1002/cmr.a.21249.

[19] Klein S and Staring M. Elastix. Edited: 2021. URL: https://github.com/SuperElastix/elastix/wiki/Home.

[20] Devaraj SJ. Chapter 2 - Emerging Paradigms in Transform-Based Medical Image Compression for Telemedicine Environment. Telemedicine Technologies. Academic Press. ISBN: 978-0-12-816948-3. Jan. 2019. URL: https://www.sciencedirect.com/science/article/pii/B9780128169483000027.

[21] Pustina D and Cook P. Anatomy of an antsRegistration call. Edited: 2021. URL: https://github.com/ANTsX/ANTs/wiki/Anatomy-of-an-antsRegistration-call.

[22] Chen DQ, Dell'Acqua F, Rokem A, Garyfallidis E, et al. Diffusion Weighted Image Co-registration: Investigation of Best Practices. BioRxiv. Dec. 2019. URL: https://www.biorxiv.org/content/10.1101/864108v2.

[23] Avants BB, Tustison NJ, Song G, Cook PA, Klein A and Gee JC. A reproducible evaluation of ANTs similarity metric performance in brain image registration. Neuroimage. Vol. 54. ISSN: 1095-9572. Feb. 2011. DOI: 10.1016/j.neuroimage.2010.09.025.

[24] Kang SK and Lee JS. Apr. 2021. DOI: 10.1088/1361-6560/abf2f7. URL: https://dx.doi.org/10.1088/1361-6560/abf2f7.

[25] Avants BB, Tustison N, and Johnson H. Advanced Normalization Tools (ANTS). July 2014. URL: https://gaetanbelhomme.wordpress.com/wp-content/uploads/2016/08/ants2.pdf.

[26] Smith SM. Fast robust automated brain extraction. Human Brain Mapping. Vol. 17. ISSN: 1065-9471. Nov. 2002. DOI: 10.1002/hbm.10062.

[27] Jenkinson M, Pechaud M, and Smith S. BET2: MR-based estimation of brain, skull and scalp surfaces. Tach. rep. TR06MP1. Oxford University Centre for Functional MRI of the Brain (FMRIB). Feb. 2006. URL: https://www.fmrib.ox.ac.uk/datasets/techrep/tr06mp1/tr06mp1.pdf.

[28] Abdi H and Williams LJ. Tukey's honestly significant difference (HSD) test. Encyclopedia of research design. Vol. 3. Num. 1. The University of Texas, Dallas. Sage Thousand Oaks, CA. 2010.

[29] Zaiontz C. Real Statistics Using Excel. Studentized Range q Table. 2023. URL: www.real-statistics.com.

[30] Igarashi KM. Entorhinal cortex dysfunction in Alzheimer's disease. Trends in Neurosciences. Vol. 46. ISSN: 1878-108X. Feb. 2023. DOI: 10.1016/j.tins.2022.11.006.

[31] Malovani C, Friedman N, Ben-Eliezer N and Tavor I. Tissue Probability Based Registration of Diffusion-Weighted Magnetic Resonance Imaging. Journal of Magnetic Resonance Imaging. Vol. 54. ISSN: 1522-2586. 2021. URL: https://onlinelibrary.wiley.com/doi/abs/10.1002/jmri.27654.

[32] Lange FJ, Arthofer C, Bartsch A, Douaud G, et al. MMORF—FSL's MultiMOdal Registration Framework. Neuroscience. preprint. Sept. 2023. DOI: 10.1101/2023.09.26.559484. URL: http://biorxiv.org/lookup/doi/10.1101/2023.09.26.559484.

A Appendix

A.1 Registration parameters

Rigid

For the registration performed with the rigid transform the following parameters were used: step size = 0.1, metric = mutual information (MI) with a weight of 1, bins = 32, sampling = Regular and sampling percentage = 0.25. The convergence = 1000 x 500 x 250 x 100 where the convergence would also be completed if 10 iterations in a row would have a change in MI-values that is below 10^{-6}. The shrink factors = 8 x 4 x 2 x 1, smoothing sigmas 3 x 2 x 1 x 0 voxels, interpolation = Linear. Then the registration was applied on the mean diffusivity image, to maintain the actual values of the MD-image but also transform it to the T1-space, with the interpolation method: LanczosWindowedSinc.

Affine

The parameters used for the registration performed with the affine transform were the exact same as the ones used for the rigid one. The same goes for how the registration was applied on the MD-image.

Nonlinear

For the registrations performed with the nonlinear transform, it was first initialized with a rigid transform which continued with a nonlinear transform called BSplineSyN. The parameters for the first part of the registration, consisting of the rigid transform, were the following: step size = 0.1, metric = Mattes which is a synonym to the mutual information metric [21]. The metric had a weighting of 1, bins = 16, sampling = Regular and sampling percentage = 0.25. Convergence = 30 x 30 x 0, where the convergence would also be completed if 10 iterations in a row would have a change in MI-values that is below 10^{-6}. The shrink factors = 3 x 2 x 1, smoothing sigmas = 2 x 1 x 0 voxels. In addition, it had a scull-stripped b:0 mask as an input as well.

The second part of the registration consisted of the nonlinear transformation with the following parameters: step size = 0.2, field mesh size at base level = 40, metric = Mattes, with a weighting of 1, bins = 16, sampling = Regular and sampling percentage = 0.25. Convergence = 20 x 20 x 0, with the convergence threshold at 10^{-6} as above. The shrink factors = 2 x 2 x 1, smoothing sigmas = 1 x 0 x 0 voxels, verbose = 1. Then the registration was applied on the mean diffusivity image, to maintain the actual values of the MD-image but also transform it to the T1-space, with the interpolation method: LanczosWindowedSinc.

Combined

The registration performed with the combined method used 3 moving images, consisting of the b:0, b:1000 and b:2500, to register against the T1-weighted image. The registration itself consisted of three parts, including a Linear interpolation and a winsorise image intensities where the lower quantile = 0.005 and the upper quantile = 0.995 in the beginning. The three parts of the registration then consisted of a rigid, affine and lastly a Syn transformation and they were applied to all of the moving images that were used as input to perform the registration. The parameters for the rigid transform were the following: step size = 0.1, metric = MI with a weighting of 1, bins = 32, sampling = Regular and sampling percentage = 0.25. Convergence = 1000 x 500 x 250 x 100, with the convergence threshold at 10^{-6} as above. The shrink factors = 8 x 4 x 2 x 1, smoothing sigmas = 3 x 2 x 1 x 0 voxels. The second part of the registration which was the affine transformation was performed with the same parameters as above.

The last part of the registration was the SyN transformation which was performed using the following parameters: step size = 0.1, metric cross correlation, with a weighting of 1 and a radius of 4. The convergence = 100 x 70 x 50 x 20, with the convergence threshold at 10^{-6} as above. The shrink factors = 8 x 4 x 2 x 1, smoothing sigmas = 3 x 2 x 1 x 0. The registration was applied on the MD-image in the same way as for the other registration methods.